The Role of Regioregularity, Crystallinity, and Chain Orientation on Electron Transport in a High-Mobility n-Type Copolymer

ARTICLE *in* JOURNAL OF THE AMERICAN CHEMICAL SOCIETY · FEBRUARY 2014

Impact Factor: 12.11 · DOI: 10.1021/ja4118736 · Source: PubMed

12 AUTHORS, INCLUDING:

Robert Steyrleuthner
Freie Universität Berlin
13 PUBLICATIONS **584** CITATIONS
SEE PROFILE

Frank Polzer
Humboldt-Universität zu Berlin
40 PUBLICATIONS **1,068** CITATIONS
SEE PROFILE

Marcel Schubert
University of St Andrews
19 PUBLICATIONS **720** CITATIONS
SEE PROFILE

Harald Werner Ade
North Carolina State University
353 PUBLICATIONS **8,627** CITATIONS
SEE PROFILE

JACS
JOURNAL OF THE AMERICAN CHEMICAL SOCIETY

Article

The Role of Regioregularity, Crystallinity and Chain Orientation on Electron Transport in a High Mobility n-type Copolymer.

Robert Steyrleuthner, Riccardo Di Pietro, Brian A. Collins, Frank Polzer, Scott Himmelberger, Marcel Schubert, Zhihua Chen, Shiming Zhang, Alberto Salleo, Harald W. Ade, Antonio Facchetti, and Dieter Neher

J. Am. Chem. Soc., **Just Accepted Manuscript** • DOI: 10.1021/ja4118736 • Publication Date (Web): 14 Feb 2014

The Role of Regioregularity, Crystallinity and Chain Orientation on Electron Transport in a High Mobility n-type Copolymer.

Robert Steyrleuthner[1], Riccardo Di Pietro[1], Brian A. Collins[2], Frank Polzer[3], Scott Himmelberger[4], Marcel Schubert[1], Zhihua Chen[5], Shiming Zhang[5], Alberto Salleo[4], Harald Ade[6], Antonio Facchetti[5]* and Dieter Neher[1]*

[1]*Universität Potsdam, Institut für Physik und Astronomie, Karl-Liebknecht-Str. 24-25, 14476 Potsdam, Germany*

[2] *National Institute of Standards and Technology, Materials Science and Engineering Division, 100 Bureau Dr., Gaithersburg, MD, 20899, USA*

[3]*Humboldt-Universität zu Berlin, Institut für Physik, Newtonstraße 15, 12489 Berlin, Germany*

[4]*Stanford University, Materials Science and Engineering, 496 Lomita Mall, Stanford, CA 94305-4034, USA*

[5]*Polyera Corporation, 8045 Lamon Ave, STE 140, Skokie, IL 60077-5318, USA*

[6]*North Carolina State University, Department of Physics, 2401 Stinson Drive, Raleigh, NC 27695, USA*

ABSTRACT: We investigate the correlation between the polymer backbone structural regularity and charge transport properties of poly{[N,N'-bis(2-octyldodecyl)-1,4,5,8-naphthalene diimide-2,6-diyl]-alt-5,5'-(2,2'-bithiophene)} (P(NDI2OD-T2)), a widely studied semiconducting polymer exhibiting high electron mobility and an unconventional micromorphology. To understand the influence of the chemical structure and crystal packing of conventional regioregular P(NDI2OD-T2) [RR-P(NDI2OD-T2)] on charge transport the corresponding regioirregular polymer [RI-P(NDI2OD-T2)] was synthesized. By combining optical, x-ray and transmission electron microscopy data we quantitatively characterize the aggregation, crystallization and backbone orientation of all polymer films, which are then correlated to electron mobilities in electron-only diodes. By carefully selecting the preparation conditions we were able to obtain RR-P(NDI2OD-T2) films with similar crystalline structure along the three crystallographic axes but with different orientation of the polymer chains with respect to the substrate surface. RI-P(NDI2OD-T2), though exhibiting a rather similar LUMO structure and energy compared to the regioregular counterpart, displayed very different packing structure, characterized by the formation of ordered stacks along the lamellar direction without detectible π-stacking. Vertical electron mobilities were extracted from the voltage and thickness dependence space-charge limited currents in unipolar devices. We demonstrate the anisotropy of charge transport along the different crystallographic axes and how mobility depends on π-stacking, but is insensitive to the degree of coherence of lamellar stacking. The comparison between the regioregular and regioirregular polymers also shows how the use of large planar functional groups leads to improved charge transport, with mobilities that are less affected by chemical and structural disorder with respect to the classic semicrystalline polymers like poly-3-hexylthiophene (P3HT).

INTRODUCTION

The development of high-mobility semiconducting polymers requires a thorough understanding of the interplay between molecular structure and solid state packing, and how they affect solid state charge transport properties[1–6]. Initial pioneering studies on alkyl substituted polythiophenes have demonstrated that tuning substitution type and degree of regioregularity, enhanced intramolecular π-conjugation, increased intermolecular π-π interactions and degree of crystallinity can substantially improve charge transport, with mobilities increasing by several orders of magnitude for highly ordered polymers[7–14]. Recent development of low band-gap polymers comprising alternating donor and acceptor (D-A) units in the backbone, on the other hand, led to an improvement of the charge transport properties, with field-effect mobilities in the range of 1 cm^2/Vs, despite showing a less ordered packing structure[15–19]. This seemingly contradictory result was primarily ascribed to the employed functional D-A units which by promoting core planarization and intermolecular π-π interactions compensate for the reduced order in the corresponding thin films[20,21].

In this respect regioregular poly{[N,N'-bis(2-octyldodecyl)-1,4,5,8-naphthalene diimide-2,6-diyl]-alt-5,5'-(2,2'-bithiophene)} (RR-P(NDI2OD-T2)), an electron transporting polymer comprising a naphthalene-diimide acceptor and a dithiophene donor units, is a very interesting system to study the correlation between molecular and solid-state structure and charge transport in donor-acceptor copolymers. Since its introduction in 2009[22], RR-P(NDI2OD-T2) has been widely utilized thanks to the facile processability and remarkable electronic properties[23–25]. A thorough characterization of this polymer revealed a rather unique film microstructure, displaying small but well-ordered crystallites with a face-on orientation in the bulk of the film, and the top surface showing an edge-on configuration[26,27]. This particular morphology allows good electron transporting properties both in vertical diodes and in field effect transistors[23,28–31]. In a recent publication we have also shown that the polymer has a strong tendency to

form well-ordered aggregates in several common organic solvents, with aggregation strongly affecting the solution and bulk optical properties[32]. The control of pre-aggregation proved to be essential for the optimization of organic solar cells, in which P(NDI2OD-T2) acts as the electron accepting component[33–37].

In an effort to understand the origin of the good transport properties of this material, Rivnay and coworkers have shown that by melt-annealing the polymer film it is possible to change the polymer chain orientation in the bulk of the film from primarily face-on to edge-on, leading to a corresponding decrease in vertical electron conductivity[38], while Schuettfort et al. have shown that the top surface is unaffected by the change of bulk orientation[27]. The strong tendency of the polymer to form ordered thin film microstructures in a wide range of processing conditions limits the possibility to analyze and separate the influence of the polymer molecular structure versus film crystallization on the electron transport properties.

In this contribution, we show the impact of several structural parameters on the electron transport of NDI-based polymers by separately tuning the chain orientation, degree of crystallinity along the different directions and degree of aggregation of the polymer chains. To achieve this goal, we synthesized for the first time a regioirregular derivative (RI-) of P(NDI2OD-T2), where the NDI-T2 linkage is random at the 2,6- and 2,7-NDI positions. On the contrary of poly(3-alkylthiophenes) such as P3HT[39,40], the regioirregular linkage does not vary the intramolecular steric demand of the backbone versus the RR-isomer (as there are no side chains on the bithienyl group), allowing this polymer to exhibit similar absorption features and LUMO level energy as its regioregular (RR-) counterpart, as shown by electrochemical and optical measurements. However, we will show that while aggregation is reduced, the RI polymer shows a rather unique microstructure comprising large, two-dimensionally ordered structures developing along the lamellar stacking and polymer backbone direction without detectible π-stacking, in striking contrast to homopolymers such as P3HT where the regioirregular linkage leads to an amorphous film with no evidence of ordering[41]. This unique feature provides us with an ideal test bench to separately study the role of ordering along the different crystallographic axes on the charge transport properties. Using either chlorobenzene, which strongly promotes aggregation in solution, or a 1:1 volume mixture of chloronaphthalene:xylene, which instead inhibits aggregation, we were able to vary both the degree of crystallinity of RR-P(NDI2OD-T2) films and the orientation of the polymer chains with respect to the substrate surface, while keeping a similar thermal history[32]. All the structural properties of the films were accessed by grazing incidence x-ray diffraction (GIXD) and transmission electron microscopy (TEM), demonstrating the role of solution pre-aggregation in the formation of well-ordered crystallites.

Finally electron-only devices were fabricated with films of RR- and RI-P(NDI2OD-T2). This provided us with the opportunity to explore the structure-charge transport correlations, demonstrating charge transport anisotropy between the lamellar and π-stacking directions. The rather high bulk electron mobility of RI-P(NDI2OD-T2) films demonstrates the role of the chemical structure of the polymer chains in improving inter-chain electron transfer, despite the poor packing registry along the π-stacking direction. Moreover, the comparison of RR- and RI-P(NDI2OD-T2) provides a direct experimental proof of the correlation between crystallization along the π-stacking direction and improved charge transport and demonstrates the insulating nature of the solubilizing side chains and the negligible influence of crystallization along the lamellar stacking direction on charge transport.

EXPERIMENTAL

Materials and Reagents. All reagents were purchased from commercial sources and used without further purification unless otherwise noted. Compound 2-octyldodecylamine[42], and 5,5'-bis(trimethylstannyl)-2,2'-bithiophene[43] were prepared according to literature procedures. Regioregular P(NDI2OD-T2) polymer[44] is now commercially available from Polyera Corporation under the trade name of ActivInk™ N2200. NMR spectra were obtained using an Inova 500 (500 MHz) NMR spectrometer. Elemental analyses were performed by Midwest microlab, LLC. Polymer molecular weights were determined on a Waters GPC system (Waters Pump 510) in THF at room temperature vs. polystyrene standards.

Preparation of 2,3,6,7-tetrabromonaphthalene-1,4,5,8-tetracarboxydianhydride (NDA-Br_4)[45]. A mixture of 1,4,5,8-naphthalenetetracarboxylic dianhydride (2.8 g, 10.3 mmol) and oleum (20 % SO_3, 100 mL) was stirred at 55 ^oC for 2 hours. A solution of dibromoisocyanuric (DBI) (6.0 g, 21.0 mmol) in oleum (50 mL) was then added over a course of 40 minutes. The resulting mixture was then warmed to 85 ^oC and maintained at this temperature for 50 hours. Upon cooling to room temperature, the reaction mixture was poured onto crushed ices (500 g). This mixture was diluted with water (500 mL) and then stirred at room temperature for 1 hour. The precipitates were collected by centrifuge, washed with water and methanol, and dried under vacuum, leading to a greenish yellow solid (6.3 g). This material was used for next step without further purification. Elemental Analysis (EA) (calc. C, 39.47; H, 0.47; N, 0.00): found C, 38.20; H, 0.79; N, 0.00.

Preparation of *N,N*'-bis(2-octyldodecyl)-2,3,6,7-tetrabromonaphthalene-1,4,5,8-bis(dicarboximide) (NDI2OD-Br_4) A mixture of NDA-Br_4 (2.34 g, 5.49 mmol), 2-octyldodecylamine (4.10 g, 13.78 mmol), *o*-xylene (18 mL), and propionic acid (6 mL) was stirred at 140 ^oC for 2 h. Upon cooling to room temperature, most of solvents were removed in vacuo, and the residue was purified by column chromatography on silica gel with a mixture of chloroform:hexane (1:1, v/v) as eluent, affording a slightly yellow solid as the product (1.98 g, 2.01 mmol, yield 36.7 %). ^1H NMR ($CDCl_3$ 500 MHz): δ (ppm): 4.13 (d, J = 7.5 Hz, 4H), 1.96 (m, 2H), 1.19-1.43 (m, 64H), 0.85-0.90 (m, 12H). EA (mass %) (calc. C, 65.84; H, 8.60; N, 2.84): found C, 65.68; H, 8.60; N, 2.89.

Preparation of *N,N*'-bis(2-octyldodecyl)-2,6&2,5-dibromonaphthalene-1,4,5,8-bis(dicarboximide) (NDI2OD-Br_2). A mixture of NDI2OD-Br_4 (2.27 g, 1.98 mmol) and Zn powder (0.32 g, 4.95 mmol) in IPA (120 mL), AcOH (10 mL) and water (5 mL) was refluxed overnight under nitrogen. After cooling to room temperature, most of the solvents were removed in vacuo, and the residue was dissolved in chloroform (~150 mL). This solution was washed with $NaHCO_3$ aqueous solution, dried over $MgSO_4$, and concentrated in vacuo. The resulting crude was first purified by column chromatography (Silica gel, dichloromethane:hexanes (2:1, v/v)) to give a mixture of 2,5 and 2,6 isomers, which was further purified by three recrystallizations from IPA to afford a

yellow solid (1.03 g, 71.0 %). ^{1}H NMR ($CDCl_3$ 500 MHz): δ (ppm): 9.01 (s, 0.68H), 8.97 (s, 0.53H), 4.16 (m, 4H), 1.97 (m, 2H), 1.20-1.40 (m, 64H), 0.84-0.89 (m, 12H). 13C NMR (CDCl3): δ (ppm):161.7, 161.5 161.3, 161.1, 139.1, 128.9, 128.6, 128.5, 127.9, 127.7, 125.4, 124.2, 45.6, 36.6, 32.1, 32.0, 31.7, 30.2, 29.9, 29.8, 29.7, 29.6, 29.5, 26.5, 22.9, 22.8, 14.3. EA (mass %) (calc. C, 65.84; H, 8.60; N, 2.84): found C, 65.64; H, 8.55; N, 2.77.

Preparation of *poly{[N,N'-bis(2-octyldodecyl)-1,4,5,8-naphthalene diimide-2,6&2,5-diyl]-alt-5,5'-(2,2'-bithiophene)} (RI-P(NDI2OD-T2).* Under argon, a mixture of NDI-2OD-Br_2 (mixture of 2,5- and 2,6-isomers) (88.4 mg, 0.090 mmol), 5,5'-bis(trimethylstannyl)-2,2'-bithiophene (38.4 mg, 0.078 mmol), and $Pd(PPh_3)_2Cl_2$ (2.7 mg, 0.0038 mmol) in anhydrous toluene (10 mL) was stirred at 90 °C for 18 hours. Bromobenzene (0.5 mL) was then added and the reaction mixture was maintained at 90 °C for an additional 5 hours. Upon cooling to room temperature, a solution of potassium fluoride (1.2 g) in water (2.4 mL) was added. This mixture was stirred at room temperature for 1 hour before it was extracted with chloroform (150 mL). The organic layer was washed with water (100 mL×2), dried over anhydrous sodium sulfate, and concentrated on a rotary evaporator. The residue was taken with chloroform (15 mL) and precipitated in methanol (100 mL) and acetone (100 mL) in sequence. The obtained blue solid product was purified by Soxhlet extraction with acetone for 48 hours. The remaining solid residue was redissolved in chloroform (20 mL) and the resulting mixture was heated to boil. Upon cooling to room temperature, the chloroform solution was filtered through a 5 μm filter, and the filtrate was added slowly to methanol (100 mL). The precipitates were collected by filtration, washed with methanol, and dried in vacuum, leading to a deep blue solid as the product (75 mg, yield 97.1 %). ^{1}H NMR ($CDCl_2CDCl_2$, 500 MHz): δ (ppm): 8.70-8.90 (m, br, 2H), 7.20-7.50 (m, br, 4H), 4.11 (s, br, 2H), 2.00 (s, br, 4H), 1.10-1.46 (m, br, 64H), 0.76-0.89 (m, br, 12H). GPC: Mn = 28.6 kg/mol. Mw = 88.5 kg/mol, PDI = 3.1. EA (mass %) (calc. C, 75.26; H, 8.96; N, 2.83): found C, 75.24; H, 8.60; N, 2.72.

Device preparation and characterization. P(NDI2OD-T2) was dissolved overnight at 60 °C using either chlorobenzene or a 1:1 mixture of chloronaphthalene:xylene (different concentrations have been used to obtain layers with different thicknesses). All the films analyzed in this work were spincoated in a nitrogen atmosphere at 1000 rpm for 30 s and rapidly transferred to a vacuum oven where they were dried at room temperature for 10 minutes. These films were either measured as such or annealed in nitrogen for 10 minutes at 200 °C. Samples for optical spectroscopy were spincoated on solvent cleaned glass (Carl Roth microscope slide 0656.1). GIXD samples were prepared on silanized doped Silicon substrates with only a native oxide coating. Samples for TEM were prepared on poly(styrenesulfonic acid) coated glass and floated onto TEM grids in deionized water. Electron-only devices were prepared by thermal evaporation of 2 nm Cs_2CO_3 at 0.1 Å/s on structured ITO (100 nm thickness and 15 Ω□ sheet resistance) at a base pressure $<2 \times 10^{-6}$ mbar and subsequent spin coating of the respective P(NDI2OD-T2) film in glovebox atmosphere. For finalizing the diode structure we applied 1 nm Cs_2CO_3 and 100 nm Aluminum (5Å/s) as top contact. Current-voltage characteristics were measured inside the glovebox by a computer-controlled Keithley 2400 source/measure unit.

Electrochemistry and Optical Absorption. Electrochemical measurements were performed on thin polymer films using a CH Instruments Model 660A electrochemical workstation with a 3-electrode cell configuration (VC-2 voltammetry cell). The solvent was dry tetrahydrofuran (THF) containing 0.1 M tetra-*n*-butylammonium hexafluorophosphate electrolyte. A 1.0 mm diameter platinum disk electrode, platinum wire counter electrode, and Ag/Ag_xO reference electrode were employed. Ferrocene/Ferrocinium (Fc/Fc^+, 0.54 V vs. saturated calomel electrode (SCE)) was used as an internal reference for all measurements, and the potential values obtained in reference to the silver electrode were converted to the saturated calomel electrode (SCE) scale (Fc/Fc^+, 0.54 V vs. SCE). Thin films were deposited onto the working electrode by drop-casting a solution of polymer sample in chloroform. The optical absorption spectra of thin films (~ 30 nm on glass) were taken with a Cary 5000 spectrometer equipped with an integrating sphere.

Grazing Incidence X-Ray Diffraction. Measurements were performed at the 7.3.3 Beamline of the Advanced Light Source (Beam energy at 10 keV and beam width ~1 mm)[46]. A Pilatus 1M photon-counting detector array was used to measure diffraction intensities. Most of the x-ray flight path was contained by a Helium atmosphere to reduce air scatter in the signal. The edges of the 2.5 cm by 2.5 cm substrates were cleaved to eliminate diffraction signal from the edge of the spincast films, leaving approximately the center 1 cm x 1 cm of the film. Diffraction intensities were acquired at an incident angle just above the film critical angle (measured to be $\alpha_C \approx 0.10^\circ$ for RR and $\alpha_C \approx 0.12^\circ$ for RI) for maximum diffraction signal and an incident angle well above the critical angle of the substrate ($\alpha = 0.20^\circ$) where intensities are linear to illuminated film volume. The results from analysis of the measurements at critical angle are presented here with their intensities scaled to those measured at the high incident angle. The intensities are additionally corrected for beam footprint (length of the sample in the beam) and film thickness.

Pole figures were constructed by integrating the intensities at each azimuth within a q-range encompassing the diffraction peak and subtracting off a linear background defined by the intensities at either end of the integrated q-range. The relative degree of crystallinity (DoC) was calculated from these pole figures by integrating the intensities over the crystallographic orientation sphere such that $DoC = \int_{0^\circ}^{90^\circ} I(\omega) sin\omega d\omega$. For the lamellar reflections, the intensities at the extreme ends of the measured range ($\omega = 1.5^\circ$ and $\omega = 85^\circ$) were extended with polynomials to fill the missing regions. Due to the larger missing regions of intensity for the π-stacking pole figures, peak functions with constant backgrounds were fit to $I(\omega)$ similar to the procedure used in[47].

For measurement of crystal spacing and coherence length, peak functions were fit to azimuthally averaged profiles $I(q)$. The azimuthal range for the average was selected based on the dominant orientation of the crystals as measured by the pole figures, which corresponded to +/-5° sector (wedge) profiles along the in- or out-of-plane scattering directions or – in the case of the lamellar diffraction from the as cast IR film – the full azimuthal range. It should be noted that the absolute π-stacking coherence lengths were highly dependent on the

chosen background, but the relative values between samples remained consistent.

Transmission Electron Microscopy. TEM specimens were prepared by floating the polymer films in deionized water onto TEM copper grids with holey carbon support film (C-Flat CF-22-2C, Protochips Inc., Raleigh, NC, USA). The carbon coated copper grids have been pre-treated for 20 seconds by glow discharge. The polymer films immobilized on the TEM grids were dried at room temperature for at least one hour. The specimens were inserted into sample holder (EM21010, JEOL GmbH, Eching, Germany) and transferred to a JEOL JEM-2100 with a LaB6 cathode (JEOL GmbH, Eching, Germany). The TEM was operated at an acceleration voltage of 200 kV. All images were recorded digitally by a bottom-mounted 4k*4k CMOS camera system (TemCam-F416, TVIPS, Gauting, Germany) and processed with a digital imaging processing system (EM-Menu 4.0, TVIPS, Gauting, Germany).

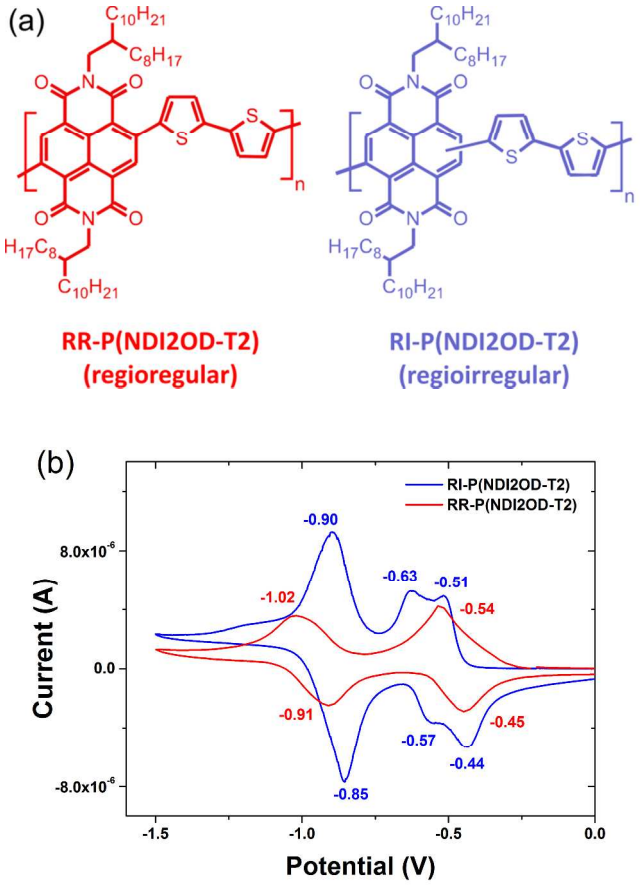

Figure 1. (a) Chemical structure of regioregular (RR) and regioirregular (RI) P(NDI2OD-T2). (b) Cyclic voltammogram of RR- and RI-P(NDI2OD-T2) referenced against SCE.

RESULTS

RI-P(NDI2OD-T2) Synthesis. The synthesis of the regioregular polymer was straightforward[44] since the key polymer building block, N,N'-bis(2-octyldodecyl)-2,6-dibromonaphthalene-1,4,5,8-bis(dicarboximide) (NDI2OD-2,6Br_2), can be easily prepared from 2,6-dibromonaphthalene-1,4,5,8-bis(dicarboximide) (NDI-Br_2), a compound which is obtained in excellent yields by brominating the corresponding anhydride (NDA). However, in order to achieve the regioirregular polymer, it is necessary either to synthesize the regiochemically pure N,N'-bis(2-octyldodecyl)-2,7-dibromonaphthalene-1,4,5,8-bis(dicarboximide) (NDI2OD-2,7Br_2), to be then mixed with NDI2OD-2,6Br_2 before polymerization with distannyldithiophene or enable a synthetic path affording the mixture of the dibrominated NDI2OD isomers. Because of the great difficulties of the former approach, we designed and carried out a route affording the isomer mixture as indicated in **Scheme 1**.

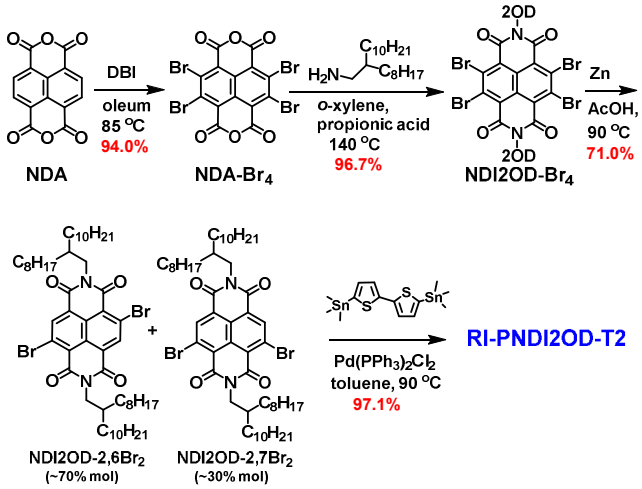

Scheme 1. Synthetic route to the regioirregular polymer.

Details of the synthesis are reported in the Experimental Section. Briefly, NDA was tetrabrominated with DBI under strong acidic conditions to afford NDA-Br_4 in good yields (94 %), which was then reacted with 2-octadecylamine to give NDI2OD-Br_4 as a pure solid after column chromatography on silica gel. Next, the tetrabromoimide system was subjected to random debromination using zinc powder, affording a mixture of brominated NDIs, from which a mixture of NDI2OD-2,6Br_2 (70 %) and NDI2OD-2,7Br_2 (30 %) was isolated after a column chromatography and multiple crystallizations. Finally, the regioirregular polymer was obtained by reacting the isomeric dibromide mixture with 5,5'-bis(trimethystannyl)-2,2'-dithiophene using $Pd(PPh_3)_2Cl_2$ as catalyst. The new polymer was purified by multiple dissolution-precipitation procedures and was characterized by EA, gel permeation chromatography (GPC) analysis, and 1H NMR spectroscopy. These systems are highly soluble in conventional organic solvents (eg > 70 mg/mL in CHCl3). The polymers used in this study have similar Mws, which are Mn = 28.6 kg/mol. Mw = 88.5 kg/mol, PDI = 3.1 for RI-P(NDI2OD-T2) and Mn = 29.3 kg/mol. Mw = 101.7 kg/mol, PDI = 3.5 for RR-P(NDI2OD-T2).

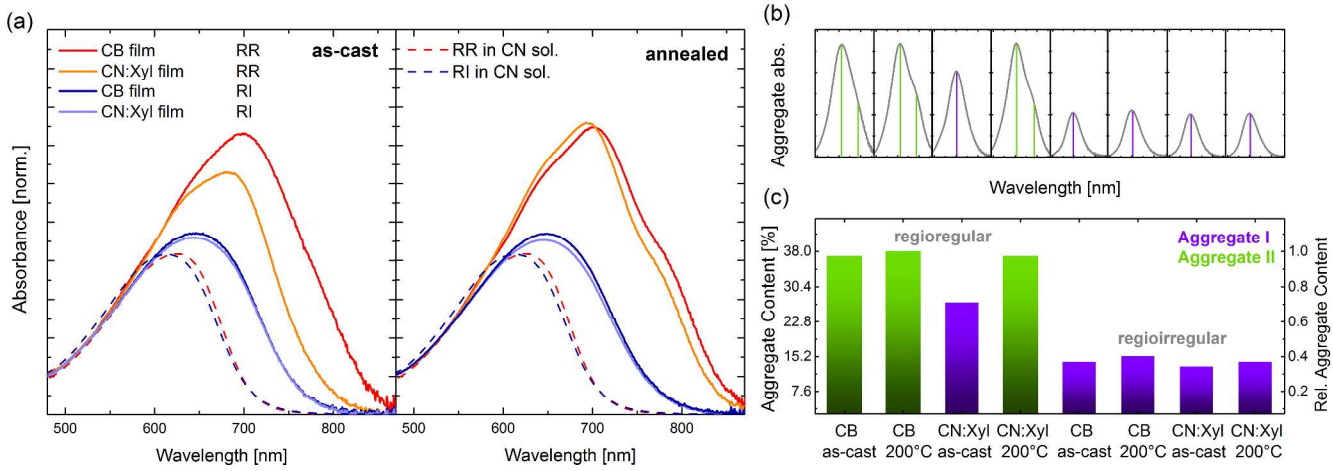

Figure 2. (a) Optical absorption of RR-P(NDI2OD-T2) and RI-P(NDI2OD-T2) thin films spincoated from the indicated solvents (CB = chlorobenzene, CN:Xyl = chloronaphthalene:xylene), as cast and after annealing for 10 minutes at 200 °C. The absorption of RR- and RI-P(NDI2OD-T2) in CN solution is reported using dashed lines, and is representative of the amorphous fraction absorption. All the spectra are normalized at 550 nm where light absorption is due only to the unaggregated polymer chains[32]. (b) Deconvolution of the amorphous and aggregate absorption features, showing the absorption of the aggregate species for the different films obtained by removing the amorphous content from Figure 2(a). The green line indicates the absorption peak at 700 nm of the aggregate I species, while the purple bars indicate the absorption peaks at 700 and 790 nm of the aggregate II species. (c) Aggregate content and type for each of the analyzed films, obtained from the ratio of amorphous to aggregate absorption intensity.

Electrochemical and optical properties. The LUMO energy levels of the RI polymer have been determined by performing cyclic voltammetry on thin films as illustrated in **Figure 1**. RI-P(NDI2OD-T2) shows three reversible reduction peaks, with the first reduction (-0.48V with respect to SCE, obtained by averaging forward (-0.51V) and reverse (-0.44V) peaks) located at a similar voltage compared to that of the RR counterpart[44]. From this data, E_{LUMO} of RI-P(NDI2OD-T2) is calculated as: - ($E_{1/2}^{red-1}$ + 4.44 eV) assuming that Koopmans' theorem holds ($EA^{red} \approx - E_{LUMO}$).[48] The LUMO energy is estimated at -3.96 eV, which is comparable to that of RR-P(NDI2OD-T2) (the calculated LUMO energy for RR-P(NDI2OD-T2) is -3.94 eV). The difference in the first reduction features in the RR and RI polymers can be explained either with the overlap of the two features in the RR polymer leading to a broader single peak, or with the presence of the regioirregular linkage (2,6 and 2,7) causing a different chemical environment and leading to a slightly different reduction feature. As far as transport is concerned however, the two peaks are very close in energy, so that the energetics of the LUMO level can be considered similar. This result together with the optical absorption spectra of both polymers in chloronaphthalene (CN) solution (dashed lines in **Figure 2a**) indicates that the electronic structure of the unaggregated polymer chains is not strongly affected by the backbone regioirregularity.

In order to obtain films with different degree of aggregation, we used our previously reported procedure, choosing either a solvent promoting aggregation in solution (chlorobenzene, CB) or a 1:1 vol. mixture by volume of chloronaphthalene:xylene (CN:Xyl), which prevents chain aggregation in solution while maintaining sufficient wetting to the substrate essential for film deposition[32,33]. We prepared films with both RR- and RI-P(NDI2OD-T2) polymers, in which we expected that the regioirregularity would reduce aggregation in solution regardless of the chosen solvent. All the films were characterized both as cast (dried in a vacuum oven at room temperature) and after post-annealing at 200 °C for 10 minutes in inert atmosphere.

The optical absorption spectra of the RR- and RI-P(NDI2OD-T2) thin films with different preparation conditions are reported as straight lines in Figure 2a. Similar to what is observed in solution (Figure S1 in the supporting information), RR-P(NDI2OD-T2) aggregation is strongly promoted in less polar solvents (going from chloronaphthalene to chlorobenzene), leading to the formation of two different aggregate species, the first one absorbing only at ~700 nm (aggregate I) and the second one exhibiting a main absorption at ~700 nm and a shoulder at ~790 nm (aggregate II)[32].

Deconvoluting the absorption spectra of the amorphous and aggregated species by removing the contribution from the amorphous fraction of the film, which shows an unstructured absorption centered at ~620 nm (dashed line in Figure 2(a), obtained from the spectrum in solution of P(NDI2OD-T2) in CN) it is possible to extract the absorption due to the aggregate species (reported in Figure 2(b), following the method reported in ref. [32]). While it is impossible to separate analytically the absorption of the two aggregate types due to the considerable overlap of their spectra, we could determine the dominant aggregate type from the presence or absence of the absorption shoulder located at ~790 nm. Comparing the oscillator strength of the amorphous and aggregate fractions in the film it is also possible to obtain the aggregate content in each of them (Figure 2(c))[49].

All the RR-P(NDI2OD-T2) films exhibit a considerable aggregate content (>25 %), with the as cast CN:Xyl film being the only one displaying exclusively aggregate I, which is consistent with using a solvent which inhibits aggregation. Thermal annealing (200 °C) of the films deposited either from CN:Xyl or from a solvent inducing pre-aggregation in solution (CB) leads to the formation of films dominated by aggregate II with a similar concentration (~35 % of the total mass), a value at which aggregation seems to saturate. Film annealing also

induces a better definition of the aggregate absorption with the sharpening of the two absorption features. Note that the aggregate content values reported here are slightly lower compared to our previous publication[32]. The absorption spectra presented in this work are measured more accurately using an integrating sphere, which removes the reflection and scattering contributions at long wavelengths.

The RI-P(NDI2OD-T2) films instead show a less structured absorption spectrum, only slightly red-shifted compared to the one of the non-aggregated polymer in CN solution. More importantly, the presence of irregular links in the polymer backbone makes the optical spectra insensitive both to the solvent used for film deposition and to the annealing conditions. However after deconvoluting the amorphous and aggregate species, all RI-P(NDI2OD-T2) films still present a significant fraction (15 %) of aggregate I species, demonstrating that even this significant structural modification of the polymer backbone is not sufficient to prevent aggregation completely.

Despite the considerable shift of the optical bandgap by over 100 nm (~0.2 eV) going from the RI- to the RR-P(NDI2OD-T2) films coated from CB, the LUMO energies obtained by cyclic voltammetry show no significant change. This result suggests that the origin of the optical shift is not caused by a further disruption of π-conjugation along the backbone of the RI polymer, as previously observed when going from RR- to RI-P3HT. For P3HT in fact head to head coupling twists the polymer backbone, affecting both HOMO and LUMO topologies and energy levels[39,40]. The regioirregular coupling in RI-P(NDI2OD-T2), due to a change from meta to para linkage in the polymer backbone, does not introduce significant additional steric constrains on the backbone planarity since both the 2,6- and 2,7- NDI-thiophene linkage have identical steric demand (identical local chemical connectivity). Furthermore, in this donor-acceptor copolymer the LUMO is strongly localized on the naphthalenediimide portion of the polymer whereas the HOMO extends throughout the central portion of the polymer involving both the NDI and thiophene units[23,25]. Consequently, the regioirregular linkage will have an asymmetric impact to the frontier molecular orbitals of these polymers, as it will cause little change to the LUMO due to localization but will impact the more extended HOMO, resulting in a wider band-gap for the RI-P(NDI2OD-T2).

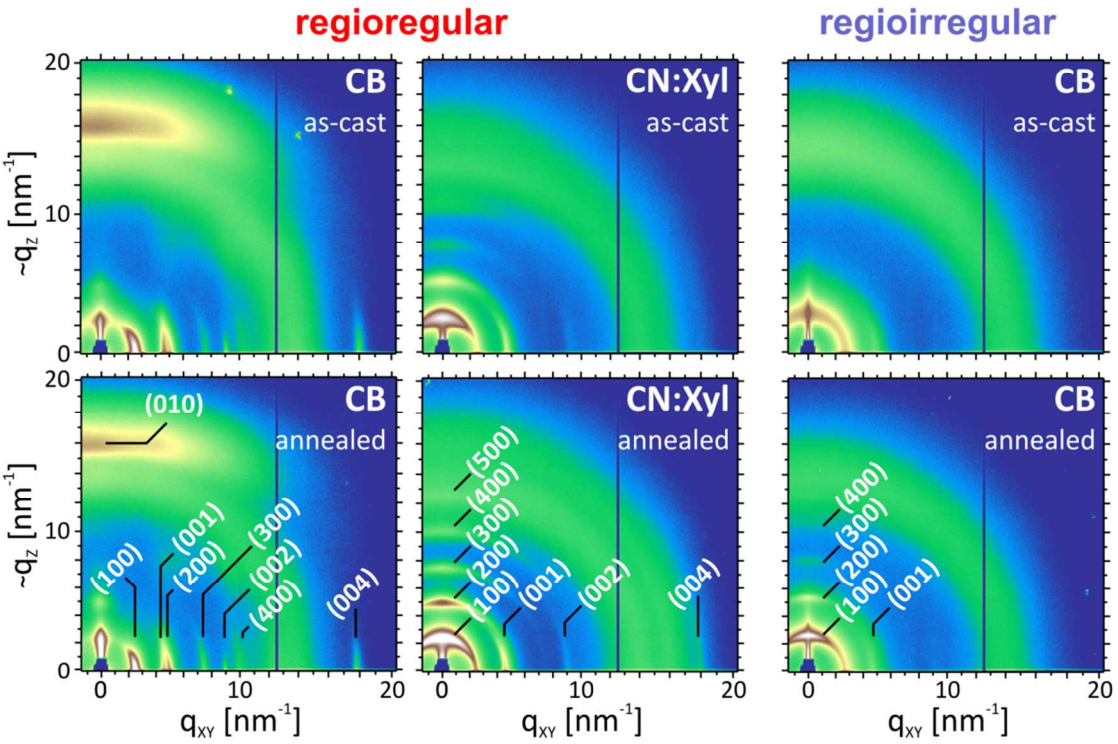

Figure 3. GIXD plot of raw 2D detector intensities for the polymer films analyzed in this study. It is of note that the q_Z-values along the vertical axis are not accurate, being distorted from curvature of the Ewald sphere. Geometrical corrections are applied for quantitative analysis in Figure 4. The peak assignments, shown in the plots, are based on previous reports[26,38,50].

Structural characterization. To investigate and quantify the microstructure of the RR and RI polymer films, we characterized them using GIXD (**Figure 3**). Since the degree of aggregation of the RI-P(NDI2OD-T2) films is independent of the chosen solvent, we limited the analysis to films prepared from CB.

GIXD plots demonstrate that the deposition solvent has a dramatic effect on the RR-P(NDI2OD-T2) film texture (crystal preferential orientation). Looking into more details at the in-plane and out-of-plane diffraction patterns it is possible to observe that the (H00) diffraction peaks (due to lamellar stacking) are present out-of-plane (~q_Z vector) for the CN:Xyl films and in-plane (q_{XY} vector) for the CB films; conversely the (010) diffraction peak is observed in-plane for CN:Xyl films and out-of-plane for the CB films. Therefore, while the crystalline fraction of the CN:Xyl films shows a preferential edge-on orientation (with the side chains aligned perpendicular to the substrate), the CB films are primarily oriented face-on with respect to the substrate surface (the (00L) peaks observed in plane in all the plots indicates that the side chains are always

lying parallel to the substrate). Although it is not possible to determine to exact tilting angles of the NDI and T2 units from these measurements, they unambiguously identify the π-orbitals stacking direction (parallel to the substrate for CN:Xyl and perdendicular to the substrate for CB). Thermal annealing increases crystalline phase content but preserves the orientation of the polymer chains in the crystallites. In the case of the annealed CB film the diffraction peaks also show a change from arcs to rods, suggesting a long range correlation of the crystallites having the same polymer orientation. This change of microstructure by using a different solvent gives access to films with similar thermal history but different polymer orientation, allowing us to separately tune degree of crystallinity and polymer chain orientation[38].

For the as-cast RI-P(NDI2OD-T2) films a rather amorphous diffraction pattern is observed, although it is possible to discern the presence of a faint diffraction peak assignable to lamellar stacking, randomly orientated with respect to the substrate. Upon thermal annealing, a significant intensity increase of the diffraction peak and the emergence of higher order reflections indicate the formation of well-ordered stacks of polymer chains aligned perpendicular to the substrate (as for the RR films deposited from CN:Xyl), substantiating the results obtained from the optical spectra: despite the regioirregular linking between the donor and acceptor units, there is still a consistent crystalline phase fraction in the film.

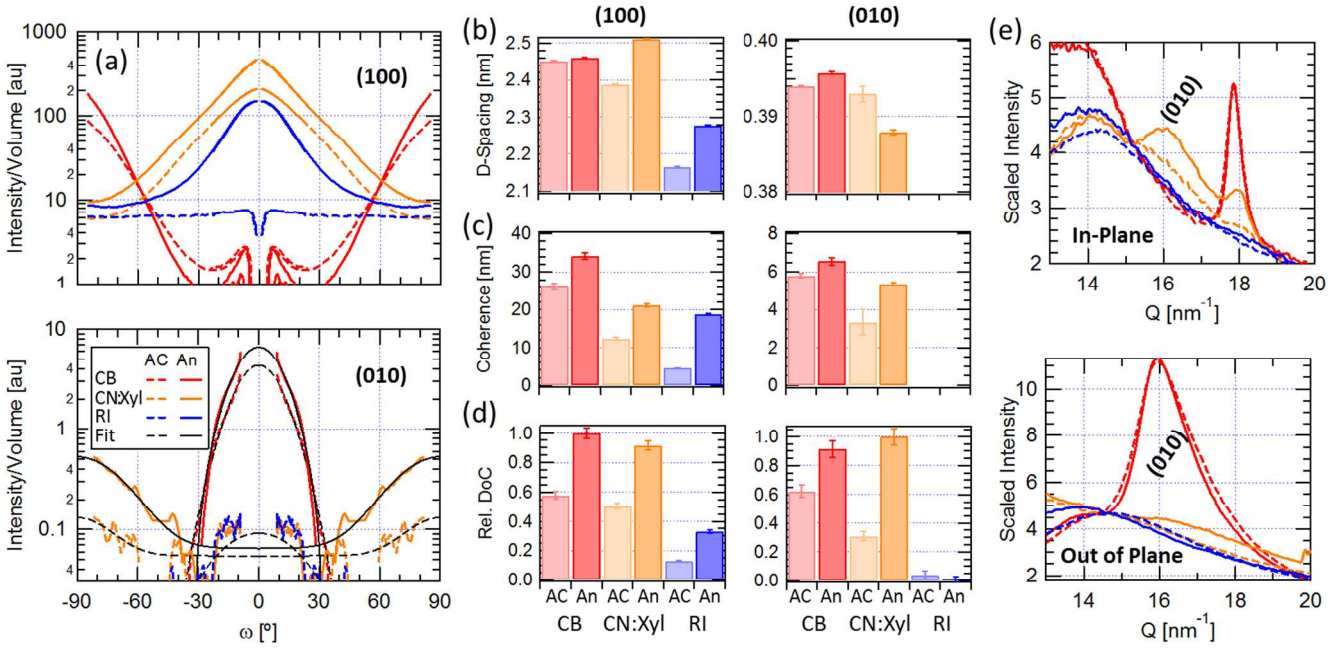

Figure 4. (a) Pole figures of the (100) (top) and (010) peaks. (b-d) d-spacing, coherence length (2π/FWHM) and relative degree of crystallinity (DoC) extracted from the first index peak for the lamellar (left) and π-stacking (right) direction. Uncertainties in (b) & (c) are uncertainties in the unweighted fit parameters. Uncertainties in (d) are from uncertainties in film thickness and sample length measurements. (e) Intensity-normalized in-plane (upper) and out-of-plane scattering profiles near the π-stacking diffraction peak at ≈16.0 nm^{-1}. AC = as-cast, An = annealed.

Calculated pole figures for the first order reflections along the lamellar- and π-stacking directions are displayed in **Figure 4(a)**[51], which represent the orientation distribution of the polymer crystals with respect to the surface normal corrected for geometrical distortions introduced by the experimental setup. The dramatic differences in crystal orientation for the regioregular polymer can easily be distinguished. Crystallites in the CB-cast films have polymer chains almost exclusively face-on while the CN:Xyl-cast films exhibit a mainly edge-on chain orientation on top of a smaller, randomly oriented population. Thermal annealing increases the orientational preference in the CB-cast film while the degree of crystallinity grows among all orientations in the CN:Xyl-cast film. The mirror-relationship of the orientational preference between the lamellar- and pi-stacking indicates that the same crystallite population is being measured in each of the pole figures. For the RI-P(NDI2OD-T2) films, the pole figure for lamellar stacking indicates a completely randomized orientation of the packed chains in the as-cast sample, while thermal annealing seems to increase only the edge-on oriented population. This result could indicate nucleation at one of the film interfaces or a preexisting edge-on population of 'amorphous' chains crystallizing upon thermal annealing. In contrast to the RR-P(NDI2OD-T2) films, while significant lamellar intensity is present in the pole figures of the regioirregular polymer film, no π-stacking intensity was observed. The small signal near $\omega = 0°$ is likely an artifact due to the assumption of a linear background. The extreme differences in crystal orientation with processing as well as the complete lack of π-stacking measured in the RI films is demonstrated in the profiles presented in Figure 4(e).

The d-spacing of both the lamellar and π-stacking directions are reported in Figure 4(b). The values measured for the RR polymer films are around 2.45 nm for the lamellar spacing and 0.39 nm for the π-stacking throughout the series, while the RI polymer films show a lower value for the lamellar spacing of 2.20 nm. Due to the missing π-stacking peak in the RI films, no information on the packing along this direction could be

obtained. The coherence length along the different directions (Figure 4(c)) shows a more significant dependence on the processing conditions, with crystallites growing both along the π- and lamellar stacking direction when using CB instead of CN:Xyl and upon annealing. It is very interesting to note how the RI-P(NDI2OD-T2) films, when annealed, show a coherence length of the lamellar stacking comparable to the one of the annealed CN:Xyl film (20 nm) indicating the formation of large, coherent lamellae despite the irregular backbone. The lamellar d-spacing also shows a general tendency to increase with the increased ordering in the film whereas the π-stacking does not. The relative degree of crystallinity (DoC) extracted from the pole plots following the procedure reported in the experimental section (Figure 4(d)) shows a similar crystallinity enhancement along the two directions, indicating that crystallite growth proceeds along both directions. The plots also clearly show the role of annealing in increasing the crystalline fraction for both RR and RI polymer films. The parameters obtained on the backbone diffraction peaks follow a very similar trend as the lamellar stacking peak except for the DoC which is found to be constant for all films (supporting information, Figure S2).

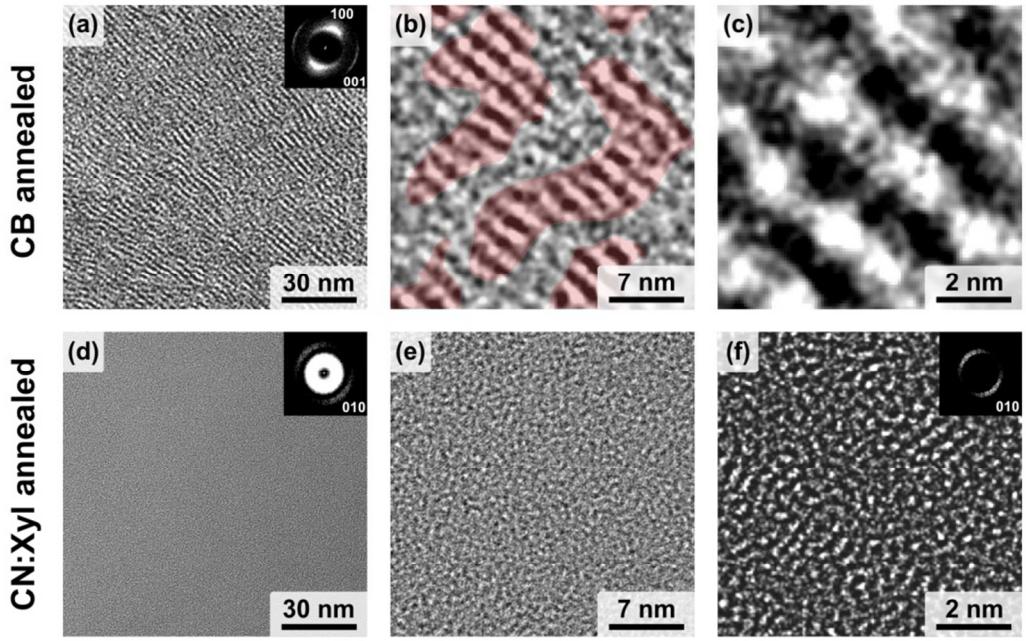

Figure 5. TEM images of P(NDI2OD-T2) prepared from CB and CN:Xyl (1:1 vol:vol), after annealing. (a) Low magnification image of CB film, which shows the aligned polymer chains lying face-on (the Fourier transform of the image, in the inset, shows two periodic features corresponding to the (100) and the (001) stacking directions). (b) Close-up of the first image, showing the aligned polymer chains: the periodic structures correspond to roughly 46 % of the area of the image. (c) High magnification image showing the stacked polymer chains. (d) Low magnification image of the CN:Xyl film, where no feature can be distinguished. The Fourier transform in the inset allows the detection of a faint periodic feature with a characteristic length corresponding to the π-π stacking. (e) Close-up of the first image, showing the difference in packing with respect to the CB film. In order to resolve the underlining periodic structure it is necessary to filter the amorphous contribution using the Fourier transform, and go to higher magnifications (f) where it is possible to observe the edge-on configuration on the substrate surface.

Transmission electron microscopy analysis. TEM allows for a closer view on the layer morphology for the different orientation of the polymer chains (**Figure 5**). In the low magnification image of the CB film (Figure 5a) the periodic structure of the stacked chains is clearly visible, while for the CN:Xyl film (Figure 5d) it is not possible to distinguish any feature. In the inset of the two images the Fourier transform of the image is shown: in the CB case two perpendicular features can be observed, with a q-vector compatible with the (100) and the (001) peaks obtained with GIXD, thus confirming the face-on configuration of the polymer chains. Furthermore, crystalline domains seem to be highly interconnected and share a long-range order on a micrometer scale, as shown, for the face-on orientation, also in the work of Takacs et al.[52], and as indicated also from the rod-shaped diffraction peaks. The FFT analysis on the CN:Xyl film shows instead only one feature, consistent with the (010) peak of the π-stacking, and a much stronger amorphous halo. At intermediate magnification (Figure 5b and 5e) it is easier to notice how the structure observed in the face-on films is absent from the edge-on films, and only by magnifying the CN:Xyl film image further (Figure 5f) and removing the amorphous content via Fourier filtering it is possible to observe the structure due to the π-stacking of the polymer chains, edge-on relative to the substrate. We finally notice that a rough estimation of the crystalline fraction obtained from the TEM image (shaded areas in Figure 5b) is consistent with the aggregate fraction determined from the optical measurements.

Aggregation vs. Crystallization. The comparison between optical and x-ray measurements provides interesting insights on the interplay between polymer aggregation and thin-film crystallinity. Let us first consider the most local parameters, the backbone (001) coherence and the degree of aggregation (DoA). The first parameter is approximately the average

length of straight chain segments, while the second measures the fraction of chains which exhibit read-shifted aggregate absorption. It has been shown before that this red-shift originates mainly from a change in backbone formation induced by inter-chain interactions in pi-stacked multi-chain assemblies[32]. We observe a strict correlation between the (001) coherence length and the DoA (Figure S3, supporting information). Given the fact that chain straightening will facilitate intimate contact between neighboring chains and, vice versa, inter-chain interaction enforces a linear chain conformation, the observed correlation is highly meaningful.

Since straight chain segments and strong π-πinteractions are inevitable for extended ordering in the π -stacking direction, samples with low 001 coherence and small DoA also exhibit low (010) DoCs and coherence. This correlation is less strict when considering the lamellar ordering. Possibly, the presence of long flexible side chains levels out, to a certain extent, backbone distortion.

The comparison of Figure 4d and in Figure 2c also reveals that the increase in DoC with annealing is stronger than the corresponding increase in DoA. This is most obvious for the CB-cast sample, which exhibits a similar DoA in the as-cast and annealed films, while annealing causes the DoC in the (100) and (010) directions to approximately double. This suggests a role for the aggregates as initiators for the formation of crystallites and that the crystallinity increase proceeds through the alignment and coalescence of multiple aggregates.

Despite the importance of aggregates for crystal formation, there is no trivial relation between the structural parameters of the crystallites as interfered from WAXS and the optical properties of the aggregate species. While Figure 2 displays two very distinct absorption features, which we assign to Aggregate I or Aggregate II, no such unique features are seen in the X-ray data. Instead, we observed a gradual increase of the (H00) and (00L) spacing with increasing order while no clear correlation with order is seen for the (0K0) spacing. Lemaur et al. calculated the change in d-spacing along the (100) direction and explained it with a change in the side chains interdigitation, which in our case could suggest a change in conformation of the polymer chains upon changing the preparation conditions[53]. However it is difficult to detect the different conformers from the d-spacing along the lamellar stacking direction only, and the changes do not correlate directly with the different aggregate types.

It has also been shown for RR-P(NDI2OD-T2) that it is possible to induce two different polymorphs denoted as Form I and Form II, where in the former one adjacent chains show a segregated structure (with donor (acceptor) units stacking on top of each other) and in latter a mixed structure (with donor units stacking on top of the acceptor units of the adjacent chain)[54]. Despite very similar d-spacing in all three crystallographic directions, these two forms could be well identified by their different 001 to 002 intensity ratio, with the mixed structure (Form II) exhibiting a highly suppressed 001 diffraction. All of our samples (including those of RI-P(NDI2OD-T2)) have similar 001 to 002 intensity ratios, with the 001 peak being more intense, meaning that they mainly consist of chains in the segregated packing (Form I).

We, therefore, propose that the optical properties of the two aggregate species are determined mainly by the backbone conformation, most likely the tilting angle between the donor and acceptor units. It is in fact known from quantum chemical calculations that the low energy absorption peak is due to an excitation from the HOMO (localized on the bithiophene unit) to the LUMO (localized on the NDI unit)[23] with a strong charge transfer character. It has also been shown how, for RR-P(NDI2OD-T2), there are two stable configuration for the relative orientation of donor and acceptor in the polymer repeating unit[28,55], one for a tilt angle of 42° and a slightly more energetically stable one for a tilt angle of 138°. This is consistent with the results we reported for calculations of the optical transitions performed on aggregated P(NDI2OD-T2) oligomers which showed a considerable redshift of the CT transition due to the reduction of the dihedral angle between the donor and the acceptor units in the polymer chains by just 10°[32]. The change in dihedral angle between the donor and acceptor units in the monomer is also observed in the work by Lemaur, where the several stable packing structures display different tilting angles between donor and acceptor. These results indicate that a change of dihedral angle between the donor and acceptor units of the monomer, in an ordered stack of the polymer chains, could be responsible for the changes in the absorption spectra of the different films. This would also explain the similar LUMO energy for both RR and RI polymer, as the regioirregular linkage would not hinder delocalization of the LUMO orbital. This is seen by the appearance of lamellar and backbone stacking with a coherence length as large as 20 nm in the annealed layer of RI-P(NDI2OD-T2), which necessitates that the NDI units can adopt a regular conformation following the strong tendency towards interdigitation of the side chains. On the other hand, always due to the regioirregular linkage, the bithiophene units will show a random tilting angles with respect to the NDI unit, therefore strongly affecting the HOMO and limiting aggregation of neighboring polymer chains in RI-P(NDI2OD-T2) while still allowing the NDI units of subsequent repeat units to exhibit the same orientation. The reason for the formation of only aggregate I in the irregular polymer, despite aggregate II being thermodynamically favourable, might be connected to the longer correlation length along the polymer backbone observed in the regioregular polymer, which might be required for the stabilization of the HOMO, and therefore not possible to achieve in the irregular polymer.

Electrical characterization. The possibility of tuning the polymer chain orientation upon solvent selection combined with the knowledge of the microstructure of the films fabricated with different conditions, and the availability of both the RR and RI polymers enable us to disentangle the role of each parameter affecting the charge transport properties of P(NDI2OD-T2). In particular RI-P(NDI2OD-T2) allows us to analyze, for the first time, a system which shows a very anisotropic crystallization, large and well defined lamellar stacking, and undetectable π-stacking, therefore addressing also the anisotropic charge transport function of the degree of ordering along the different crystallographic directions.

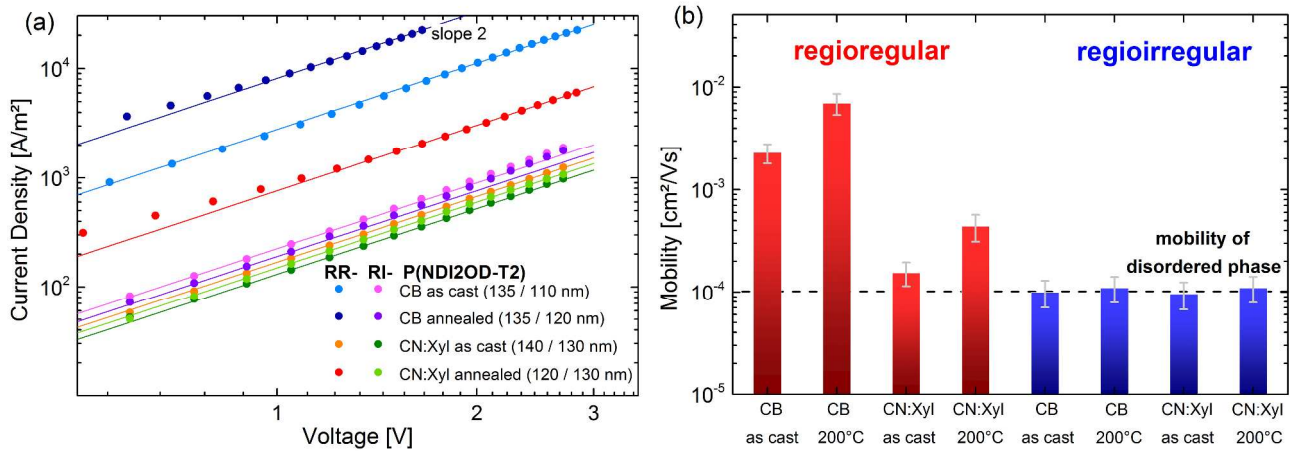

Figure 6. (a) *J-V* curves (only one in three data point is shown for clarity) of electron only diodes with RR- and RI-P(NDI2OD-T2): the films spun from chlorobenzene show the highest conductivity, while the chloronaphthalene:xylene ones have worse performance. The lines are fit to the experimental data using the standard trap-free SCLC equation, with a fixed slope of 2, expected from a quadratic dependence of the current on the applied voltage. (b) Extracted mobilities using the SCLC formalism: in blue are reported the values obtained from the regio-irregular polymer, while in red are the results obtained from the regio-regular one. Error bars are obtained by averaging several devices on each substrate and taking into account the uncertainty on the thickness measurements.

In order to extract the electron mobility, we realized space charge limited current (SCLC) diodes with the same preparation conditions of the films used for the structural characterization. The current-voltage characteristics for these devices are reported in **Figure 6a** (the full J-V characteristics, including the low voltage part of the plot which shows an ohmic behavior, are shown in Figure S4 for devices prepared from RR-P(NDI2OD-T2)). As can be seen from the plot, all the curves show for most of the voltage range a quadratic dependence of the current on the applied voltage. While we originally showed that electron injection into P(NDI2OD-T2) from typical cathodes (Ca, Ba, Sm and CsF) is contact-limited[31], Wetzelear et al recently demonstrated ohmic injection for this material by using cesium carbonate as top contact[28]. Inspired by this work, we used Cs_2CO_3 as top and bottom contact in order to prevent the oxidation of the bottom aluminum electrode upon heat treatment.

The SCLC mobility $\boldsymbol{\mu}$ was extracted using the standard trap-free SCLC transport equation:

$$J = \frac{9}{8}\varepsilon_r\varepsilon_0\mu\frac{U^2}{d^3}$$

where $\boldsymbol{\varepsilon_r}$ is the relative dielectric constant, $\boldsymbol{\varepsilon_0}$ is the vacuum permeability, $\boldsymbol{U}$ is the applied voltage, and $\boldsymbol{d}$ is the device thickness. The validity of the extraction method was confirmed by ensuring that the current across devices with different thicknesses scaled following a $\boldsymbol{d^3}$ dependence (Figure S5, supporting information). The extracted mobilities are reported in Figure 6b.

The most obvious correlation is between chain orientation and mobility. Notably, though having a lower DoC in the lamellar and pi-stacking direction, the mobility of the pristine CB-coated sample with face-on orientation is almost 10 times higher than of the annealed CN:Xy-cast film with an edge-on morphology. This confirms the importance of coherent π-stacking along the direction of charge transport for reaching extraordinary high electron mobilities with this polymer. The threefold increase in mobility upon annealing of the CB-coated sample is correlated with the increase in DoC, indicating the formation of more or larger crystalline domains from the aggregate species. Interestingly, annealing the edge-on oriented samples also results in an approximate threefold increase in mobility. While one might be tempted to attribute this simply to the transition from Aggregate I to Aggregate II, we notice the large increase in both the degree of crystallinity and of coherence length along the π-stacking direction upon annealing. The concurrent improvement of in-plane transport will provide better access to pathways for charge transport along the vertical direction[56]. Our proposal is that the π-stacking coherence and not the quality of packing in the lamellar direction is important for efficient vertical transport also in case of edge-on chain orientation.

This view is fully confirmed by the electrical properties of RI-P(NDI2OD-T2). Despite the fact that annealing leads to a considerable increase of the coherence and DoC in the lamellar direction of that sample, the vertical mobility is not affected. Given the lack of any order along the π-stacking direction, this result is a clear indication of how the increase in coherence length and DoC along the lamellar stacking direction has no impact on the electron transport properties.

Finally, we note that even the as cast RI-P(NDI2OD-T2), which has a very low DoC in any direction, shows a surprisingly high mobility when compared with other regio-irregular polymers such as RI-P3HT[12,57]. In particular, a close look at the shape of the SCLC curves reveals a clear quadratic dependence for all the different devices, both with RR and RI polymer. The similarity of the different traces indicates that apart for a general decrease of the electron mobility, the energetic landscape for both RR- and RI-P(NDI2OD-T2) is very similar and characterized also in the more amorphous films by a very small energetic disorder[58].

This corroborates the hypothesis that the LUMO is not strongly changed upon aggregation, as already discussed in the previous section, so that while charge transfer is enhanced by the increase of DoC along the π-stacking direction, the energetic structure of the LUMO is not. The reason is twofold. The regio-random coupling in P3HT has a direct impact on conjugation length due to steric constrains, as it inhibits planarization of the backbone thus dramatically affecting the energetic structure of the polymer film. This is not true for regio-random

coupling in P(NDI2OD-T2) where the irregular linking does not cause the same steric hindrance issues. For the latter polymer the main effect seems to be related to the inhibition of π-stacking, while the energetics of the LUMO level is not strongly affected by the presence of irregular linking, as shown from the electrochemical data. Moreover, according to quantum chemical calculations, negative charges in P(NDI2OD-T2) are delocalized over a small number of repeating units compared to polymers such as P3HT[23]. Combined with the larger and more planar repeating units adopted in this high mobility polymer it leads to a structure which is more tolerant to disorder and provides a higher baseline for charge transport regardless of the film microstructure[59].

CONCLUSIONS.

In conclusion, by analyzing and comparing optical, structural and charge transport information this work shows some peculiar properties of donor-acceptor NDI-copolymers.

In order to study the role of solid state morphology and microstructure on the charge transport properties of regioregular P(NDI2OD-T2), we prepared thin films using different solvents to tune the degree of aggregation in solution. The thin-film structural characterization revealed that the different solvents have a dramatic impact on the orientation of the polymer chains with respect to the substrate, allowing us to achieve edge-on and face-on microstructured films without thermal annealing of the polymer films above the melting temperature.

By measuring of the vertical electron mobility in unipolar diodes of these devices, crystallinity along the π-stacking direction is identified to be highly important for achieving high electron mobilities. On the other hand, the side chains create a barrier for electron transfer, demonstrating how lamellar ordering plays a subordinate role in electron transport. The anisotropy of the charge transport properties is confirmed by the effect of chain orientation in the RR polymer films, where vertical diodes comprising films with face-on morphology display one order of magnitude increase in electron mobility compared with diodes prepared with films having an edge-on polymer conformation.

We also reported a new synthetic route to obtain a regioirregular version of P(NDI2OD-T2), which shows a similar LUMO energy as the regioregular counterpart, and a lower degree of aggregation, which is however still involving ~ 10 % of the total polymer mass. Surprisingly, this polymer shows anisotropic packing structure, with the formation of well-ordered lamellar stacks but without measurable π-stacking. Due to the fact that there are no side chains attached to the bithiophene units, irregular linkage will increase backbone steric demand between the large NDI units, despite a random orientation of the bithiophene units. This is different from regioirregular P3HT where the different absorption and much lower mobility compared to regioregular P3HT has been attributed to steric constraints. As a consequence, we observe a rather small difference in mobility between RR- and RI-P(NDI2OD-T2). This result demonstrates how the use of larger planar units can indeed improve the charge transfer process, making it more resilient to the increased disorder introduced by the regioirregular linking, and providing a higher baseline mobility regardless of the microstructure of the polymer film.

ASSOCIATED CONTENT

Supporting Information. The spectra of the RR- and RI-P(NDI2OD-T2) in different solvents are reported as Figure S1, the analysis of the backbone diffraction peaks as Figure S2, the correlation between backbone diffraction peak coherence length and aggregate content as Figure S3. The full I-V plots, including the ohmic part of the curves are reported in Figure S4 and the thickness dependence analysis of the SCLC curves is reported in figure S5. This material is available free of charge via the Internet at http://pubs.acs.org.

AUTHOR INFORMATION

Corresponding Authors

a-facchetti@northwestern.edu
neher@uni-potsdam.de

Author Contributions

The manuscript was written through contributions of all authors.

Funding Sources

Dr. Frank Polzer would like to thank the CRC 951 of the Deutsche Forschungsgemeinschaft (DFG) and the Joint Lab for Structural Research Berlin for founding. Marcel Schubert acknowledges funding by the DFG within the SPP 1355. B. A. Collins acknowledges financial support of the NIST-NRC post-doctoral fellowship program. HA is supported by DOE, OS, BES, MSE (DE-FG02-98ER45737). GIXD data was acquired at beamline 7.3.3, of the ALS, a National user facility supported by DOE (DE-AC02-05CH1123). Part of this work was funded by the German Federal Ministry of Science and Education (BMBF FKZ 03X3525D) within SOHyb (FKZ 03X3525D). D.N. thanks the DFG for a travel grant. This work was financially supported by the Deutsche Forschungsgemeinschaft (DFG) within the Collaborative Research Centre HIOS (SFB 951).

ACKNOWLEDGMENT

The authors would like to acknowledge Gert-Jan Wetzelaer and Jan-Anton Koster for help in the preparation of the SCLC diodes used in this work, and Dr. Holm Kirmse for fruitful discussion concerning the TEM results.

REFERENCES

(1) Donley, C. L.; Zaumseil, J.; Andreasen, J. W.; Nielsen, M. M.; Sirringhaus, H.; Friend, R. H.; Kim, J. *J. Am. Chem. Soc.* **2005**, *127*, 12890–12899.

(2) Salleo, A. *Mater. Today* **2007**, *10*, 38–45.

(3) McCulloch, I.; Heeney, M.; Bailey, C.; Genevicius, K.; Macdonald, I.; Shkunov, M.; Sparrowe, D.; Tierney, S.; Wagner, R.; Zhang, W.; Chabinyc, M. L.; Kline, R. J.; McGehee, M. D.; Toney, M. F. *Nat. Mater.* **2006**, *5*, 328–33.

(4) Cadby, A. J.; Lane, P. A.; Mellor, H.; Martin, S. J.; Grell, M.; Giebeler, C.; Bradley, D. D. C.; Wohlgenannt, M.; An, C.; Vardeny, Z. V. *Phys. Rev. B* **2000**, *62*, 15604–15609.

(5) Guo, X.; Zhou, N.; Lou, S. J.; Smith, J.; Tice, D. B.; Hennek, J. W.; Ortiz, R. P.; Navarrete, J. T. L.; Li, S.; Strzalka, J.; Chen, L. X.; Chang, R. P. H.; Facchetti, A.; Marks, T. J. *Nat. Photonics* **2013**, *7*, 815–833.

(6) Facchetti, A. *Chem. Mater.* **2011**, *23*, 733–758.

(7) Sirringhaus, H.; Brown, P. J.; Friend, R. H.; Nielsen, M. M.; Bechgaard, K.; Langeveld-Voss, B. M. W.; Spiering, A. J. H.; Janssen, R. A. J.; Meijer, E. W.; Herwig, P.; de Leeuw, D. M. *Nature* **1999**, *401*, 685–688.

(8) Zen, A.; Pflaum, J.; Hirschmann, S.; Zhuang, W.; Jaiser, F.; Asawapirom, U.; Rabe, J. P.; Scherf, U.; Neher, D. *Adv. Funct. Mater.* **2004**, *14*, 757–764.

(9) Kline, R. J.; McGehee, M. D.; Kadnikova, E. N.; Liu, J.; Fréchet, J. M. J. *Adv. Mater.* **2003**, *15*, 1519–1522.

(10) Jimison, L. H.; Toney, M. F.; McCulloch, I.; Heeney, M.; Salleo, A. *Adv. Mater.* **2009**, *21*, 1568–1572.

(11) Sirringhaus, H.; Tessler, N.; Friend, R. H. *Science* **1998**, *280*, 1741–1744.

(12) Bao, Z.; Dodabalapur, A.; Lovinger, A. J. *Appl. Phys. Lett.* **1996**, *69*, 4108.

(13) Crossland, E. J. W.; Tremel, K.; Fischer, F.; Rahimi, K.; Reiter, G.; Steiner, U.; Ludwigs, S. *Adv. Mater.* **2012**, *24*, 839–44.

(14) Luzio, A.; Fazzi, D.; Natali, D.; Giussani, E.; Baeg, K.-J.; Chen, Z.; Noh, Y.-Y.; Facchetti, A.; Caironi, M. *Adv. Funct. Mater.* **2013**, *[Online Early Access]* DOI: 10.1002/adfm.201302297. Published Online: 29 OCT 2013.

(15) Chen, H.; Guo, Y.; Yu, G.; Zhao, Y.; Zhang, J.; Gao, D.; Liu, H.; Liu, Y. *Adv. Mater.* **2012**, *24*, 4618–22.

(16) Chen, Z.; Lee, M. J.; Shahid Ashraf, R.; Gu, Y.; Albert-Seifried, S.; Nielsen, M. M.; Schroeder, B.; Anthopoulos, T. D.; Heeney, M.; McCulloch, I.; Sirringhaus, H. *Adv. Mater.* **2011**, *24*, 647–652.

(17) Van Hal, P. A.; Smits, E. C. P.; Geuns, T. C. T.; Akkerman, H. B.; De Brito, B. C.; Perissinotto, S.; Lanzani, G.; Kronemeijer, A. J.; Geskin, V.; Cornil, J.; Blom, P. W. M.; De Boer, B.; De Leeuw, D. M. *Nat. Nanotechnol.* **2008**, *3*, 749–754.

(18) Kronemeijer, A. J.; Gili, E.; Shahid, M.; Rivnay, J.; Salleo, A.; Heeney, M.; Sirringhaus, H. *Adv. Mater.* **2012**, *24*, 1558–1565.

(19) Tsao, H. N.; Cho, D. M.; Park, I.; Hansen, M. R.; Mavrinskiy, A.; Yoon, D. Y.; Graf, R.; Pisula, W.; Spiess, H. W.; Müllen, K. *J. Am. Chem. Soc.* **2011**, *133*, 2605–2612.

(20) Lu, G.; Blakesley, J.; Himmelberger, S.; Pingel, P.; Frisch, J.; Lieberwirth, I.; Salzmann, I.; Oehzelt, M.; Di Pietro, R.; Salleo, A.; Koch, N.; Neher, D. *Nat. Commun.* **2013**, *4*, 1588–1596.

(21) Zhang, X.; Bronstein, H.; Kronemeijer, A. J.; Smith, J.; Kim, Y.; Kline, R. J.; Richter, L. J.; Anthopoulos, T. D.; Sirringhaus, H.; Song, K.; Heeney, M.; Zhang, W.; McCulloch, I.; DeLongchamp, D. M. *Nat. Commun.* **2013**, *4*, 2238.

(22) Yan, H.; Chen, Z.; Zheng, Y.; Newman, C.; Quinn, J. R.; Dötz, F.; Kastler, M.; Facchetti, A. *Nature* **2009**, *457*, 679–686.

(23) Caironi, M.; Bird, M.; Fazzi, D.; Chen, Z.; Di Pietro, R.; Newman, C.; Facchetti, A.; Sirringhaus, H. *Adv. Funct. Mater.* **2011**, *21*, 3371–3381.

(24) Baeg, K.-J.; Khim, D.; Jung, S.-W.; Kang, M.; You, I.-K.; Kim, D.-Y.; Facchetti, A.; Noh, Y.-Y. *Adv. Mater.* **2012**, *24*, 5433–5439.

(25) Fazzi, D.; Caironi, M.; Castiglioni, C. *J. Am. Chem. Soc.* **2011**, *133*, 19056–19059.

(26) Rivnay, J.; Toney, M. F.; Zheng, Y.; Kauvar, I. V.; Chen, Z.; Wagner, V.; Facchetti, A.; Salleo, A. *Adv. Mater.* **2010**, *22*, 4359–4363.

(27) Schuettfort, T.; Thomsen, L.; McNeill, C. R. *J. Am. Chem. Soc.* **2012**, *135*, 1092–1101.

(28) Wetzelaer, G.-J. A. H.; Kuik, M.; Olivier, Y.; Lemaur, V.; Cornil, J.; Fabiano, S.; Loi, M. A.; Blom, P. W. M. *Phys. Rev. B* **2012**, *86*, 165203.

(29) Fabiano, S.; Musumeci, C.; Chen, Z.; Scandurra, A.; Wang, H.; Loo, Y.-L.; Facchetti, A.; Pignataro, B. *Adv. Mater.* **2012**, *24*, 951–956.

(30) Fabiano, S.; Yoshida, H.; Chen, Z.; Facchetti, A.; Loi, M. A. *ACS Appl. Mater. Interfaces* **2013**, *5*, 4417–4422.

(31) Steyrleuthner, R.; Schubert, M.; Jaiser, F.; Blakesley, J. C.; Chen, Z.; Facchetti, A.; Neher, D. *Adv. Mater.* **2010**, *22*, 2799–2803.

(32) Steyrleuthner, R.; Schubert, M.; Howard, I.; Klaumünzer, B.; Schilling, K.; Chen, Z.; Saalfrank, P.; Laquai, F.; Facchetti, A.; Neher, D. *J. Am. Chem. Soc.* **2012**, *134*, 18303–18317.

(33) Schubert, M.; Dolfen, D.; Frisch, J.; Roland, S.; Steyrleuthner, R.; Stiller, B.; Chen, Z.; Scherf, U.; Koch, N.; Facchetti, A.; Neher, D. *Adv. Energy Mater.* **2012**, *2*, 369–380.

(34) Facchetti, A. *Mater. Today* **2013**, *16*, 123–132.

(35) Zhou, N.; Lin, H.; Lou, S. J.; Yu, X.; Guo, P.; Manley, E. F.; Loser, S.; Hartnett, P.; Huang, H.; Wasielewski, M. R.; Chen, L. X.; Chang, R. P. H.; Facchetti, A.; Marks, T. J. *Adv. Energy Mater.* **2013**, *[Online Early Access]* DOI: 10.1002/aenm.201300785. Published Online: 2 OCT 2013.

(36) Tang, Y.; McNeill, C. R. *J. Polym. Sci. Part B Polym. Phys.* **2013**, *51*, 403–409.

(37) Mori, D.; Benten, H.; Okada, I.; Ohkita, H.; Ito, S. *Adv. Energy Mater.* **2013**, *[Online Early Access]* DOI: 10.1002/aenm.201301006. Published Online: 2 OCT 2013.

(38) Rivnay, J.; Steyrleuthner, R.; Jimison, L. H.; Casadei, A.; Chen, Z.; Toney, M. F.; Facchetti, A.; Neher, D.; Salleo, A. *Macromolecules* **2011**, *44*, 5246–5255.

(39) Ko, S.; Hoke, E. T.; Pandey, L.; Hong, S.; Mondal, R.; Risko, C.; Yi, Y.; Noriega, R.; McGehee, M. D.; Brédas, J.-L.; Salleo, A.; Bao, Z. *J. Am. Chem. Soc.* **2012**, *134*, 5222–5232.

(40) Tsoi, W. C.; Spencer, S. J.; Yang, L.; Ballantyne, A. M.; Nicholson, P. G.; Turnbull, A.; Shard, A. G.; Murphy, C. E.; Bradley, D. D. C.; Nelson, J.; Kim, J.-S. *Macromolecules* **2011**, *44*, 2944–2952.

(41) Wang, C.; Rivnay, J.; Himmelberger, S.; Vakhshouri, K.; Toney, M. F.; Gomez, E. D.; Salleo, A. *ACS Appl. Mater. Interfaces* **2013**, *5*, 2342–6.

(42) Letizia, J. A.; Salata, M. R.; Tribout, C. M.; Facchetti, A.; Ratner, M. A.; Marks, T. J. *J. Am. Chem. Soc.* **2008**, *130*, 9679–9694.

(43) Goto, H.; Akagi, K. *Angew. Chemie* **2005**, *44*, 4322432–8.

(44) Chen, Z.; Zheng, Y.; Yan, H.; Facchetti, A. *J. Am. Chem. Soc.* **2009**, *131*, 8–9.

(45) Röger, C.; Würthner, F. *J. Org. Chem.* **2007**, *72*, 8070–8075.

(46) Hexemer, A.; Bras, W.; Glossinger, J.; Schaible, E.; Gann, E.; Kirian, R.; MacDowell, A.; Church, M.; Rude, B.; Padmore, H. *J. Phys. Conf. Ser.* **2010**, *247*, 012007.

(47) Duong, D. T.; Toney, M. F.; Salleo, A. *Phys. Rev. B* **2012**, *86*, 205205.

(48) Bard, A. J.; Faulkner, L. R. *Electrochemical Methods - Fundamentals and Applications*; WILEY: New York, 1980.

(49) Clark, J.; Chang, J.-F.; Spano, F. C.; Friend, R. H.; Silva, C. *Appl. Phys. Lett.* **2009**, *94*, 163306.

(50) Rivnay, J.; Noriega, R.; Kline, R. J.; Salleo, A.; Toney, M. F. *Phys. Rev. B* **2011**, *84*, 045203.

(51) Baker, J. L.; Jimison, L. H.; Mannsfeld, S.; Volkman, S.; Yin, S.; Subramanian, V.; Salleo, A.; Alivisatos, A. P.; Toney, M. F. *Langmuir* **2010**, *26*, 9146–9151.

(52) Takacs, C. J.; Treat, N. D.; Kraemer, S.; Chen, Z.; Facchetti, A.; Chabinyc, M. L.; Heeger, A. J. *Nano Lett.* **2013**, *13*, 2522–2527.

(53) Lemaur, V.; Muccioli, L.; Zannoni, C.; Beljonne, D.; Lazzaroni, R.; Cornil, J.; Olivier, Y. *Macromolecules* **2013**, *46*, 8171–8178.

(54) Brinkmann, M.; Gonthier, E.; Bogen, S.; Tremel, K.; Ludwigs, S.; Hufnagel, M.; Sommer, M. *ACS Nano* **2012**, *6*, 10319–10326.

(55) Giussani, E.; Fazzi, D.; Brambilla, L.; Caironi, M.; Castiglioni, C. *Macromolecules* **2013**, *46*, 2658–2670.

(56) Tessler, N.; Preezant, Y.; Rappaport, N.; Roichman, Y. *Adv. Mater.* **2009**, *21*, 2741–2761.

(57) Assadi, A.; Svensson, C.; Willander, M.; Ingana□s, O. *Appl. Phys. Lett.* **1988**, *53*, 195.

(58) Nicolai, H. T.; Mandoc, M.; Blom, P. W. M. *Phys. Rev. B* **2011**, *83*, 195204.

(59) Noriega, R.; Rivnay, J.; Vandewal, K.; Koch, F. P. V; Stingelin, N.; Smith, P.; Toney, M. F.; Salleo, A. *Nat. Mater.* **2013**, *12*, 1038–1044.

TOC

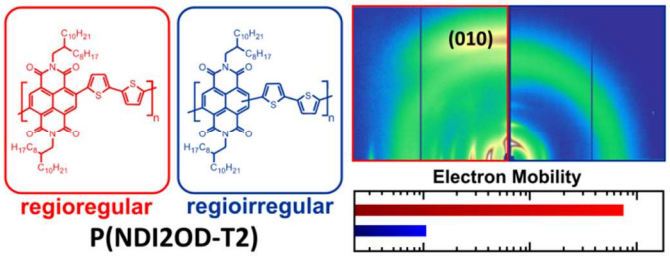
regioregular
regioirregular
P(NDI2OD-T2)
(010)
Electron Mobility